

(d) Estimated equilibrium (r_e) C–H bond lengths

The corrected C–H bond lengths from neutron diffraction as described above are of interest because they are estimated equilibrium (r_e) values, comparable with those determined theoretically and from other experimental methods (Kuchitsu & Oyanagi, 1977). Thus for C–H in ethane, theoretical calculations with an extended basis set, including electron correlation effects (MP2/6-31G*) give the value 1.094 Å (DeFrees, Levi, Pollock, Hehre, Binkley & Pople, 1979). Corresponding experimental values for ethane are 1.0877 Å from infrared spectra (Duncan, McKean & Bruce, 1979), 1.0940(2) Å from microwave spectra (Hirota, Endo, Saito & Duncan, 1981) and 1.089(5) Å from gas electron diffraction. The latter is an r_e value derived by Duncan *et al.* (1979) from the results of Bartell & Higginbotham (1965). These experimental C–H bond lengths, including the ten from neutron diffraction, lie within a range of 0.015 Å which is centered on the theoretical value.

The greater part of this work was carried out at Brookhaven National Laboratory, under contract with the US Department of Energy. It was also supported by NIH Grants GM-22548 and HL-20350. H-PW thanks the Humboldt Foundation, Federal Republic of Germany, for partial support. We are indebted to Joseph Henriques and Mrs Joan Klinger for their technical assistance.

References

- BARTELL, L. S. & HIGGINBOTHAM, H. K. (1965). *J. Chem. Phys.* **42**, 851–856.
 BECKER, P. J. & COPPENS, P. (1974). *Acta Cryst.* **A30**, 129–147.

- BUSING, W. R., MARTIN, K. O. & LEVY, H. A. (1962). *ORFLS*. Report ORNL-TM-305. Oak Ridge National Laboratory, Tennessee.
 CRAVEN, B. M. & HE, X.-M. (1982). *Programs for Thermal Motion Analysis*, Tech. Rep., Department of Crystallography, Univ. of Pittsburgh.
 DEFREES, D. J., LEVI, B. A., POLLOCK, S. K., HEHRE, W. J., BINKLEY, J. S. & POPLE, J. A. (1979). *J. Am. Chem. Soc.* **101**, 4085–4087.
 DETITTA, G. T. & CRAVEN, B. M. (1973). *Acta Cryst.* **B29**, 1354–1357.
 DUNCAN, J. L., MCKEAN, D. C. & BRUCE, A. J. (1979). *J. Mol. Spectrosc.* **74**, 361–374.
 DUNITZ, J. D. & WHITE, D. N. J. (1973). *Acta Cryst.* **A29**, 93–94.
 HIROTA, E., ENDO, Y., SAITO, S. & DUNCAN, J. L. (1981). *J. Mol. Spectrosc.* **89**, 285–295.
 HITCHCOCK, P. B., MASON, R., THOMAS, K. M. & SHIPLEY, G. G. (1974). *Proc. Natl Acad. Sci. USA*, **71**, 3036–3040.
 IBERS, J. A. (1959). *Acta Cryst.* **12**, 251–252.
 JOHNSON, C. K. (1976). *ORTEPII*. Report ORNL-5138. Oak Ridge National Laboratory, Tennessee.
 KOESTER, L. (1977). *Neutron Physics*, edited by G. HOHLER, p. 1. Berlin: Springer.
 KRAUT, J. (1961). *Acta Cryst.* **14**, 1146–1152.
 KUCHITSU, K. & BARTELL, L. S. (1961). *J. Chem. Phys.* **35**, 1945–1949.
 KUCHITSU, K. & OYANAGI, K. (1977). *Faraday Discuss. Chem. Soc.* **62**, 20–28.
 MCMULLAN, R. K. & KOETZLE, T. F. (1979). Unpublished.
 MEULENAER, J. DE & TOMPA, H. (1965). *Acta Cryst.* **19**, 1014–1018.
 SCHOMAKER, V. & TRUEBLOOD, K. N. (1968). *Acta Cryst.* **B24**, 63–76.
 SUNDARALINGAM, M. (1968). *Nature (London)*, **217**, 35–37.
 SUNDARALINGAM, M. (1969). *Biopolymers*, **7**, 821–860.
 SUNDARALINGAM, M. & PUTKEY, E. F. (1970). *Acta Cryst.* **B26**, 790–799.
 SWAMINATHAN, S. & CRAVEN, B. M. (1984). *Acta Cryst.* **B40**, 511–518.
 TEMPLETON, L. K. & TEMPLETON, D. H. (1973). *Abstr. Am. Crystallogr. Assoc. Meet.*, Storrs, CT, p. 143.
 WEBER, H.-P., CRAVEN, B. M. & MCMULLAN, R. K. (1983). *Acta Cryst.* **B39**, 360–366.

Acta Cryst. (1984). **B40**, 511–518

Electrostatic Properties of Phosphorylethanolamine at 123 K from Crystal Diffraction

BY S. SWAMINATHAN AND B. M. CRAVEN

Department of Crystallography, University of Pittsburgh, Pittsburgh, PA 15260, USA

(Received 15 December 1983; accepted 6 March 1984)

Abstract

Electrostatic properties for phosphorylethanolamine ($C_2H_8NO_4P$) at 123 K have been determined from X-ray (Mo $K\alpha$) intensity data (4150 reflections with $|F_o| \geq 3\sigma$ and $\sin \theta/\lambda < 1.3 \text{ \AA}^{-1}$). Least-squares structure refinements were carried out using Stewart's rigid pseudoatom model (at convergence $R = 0.029$, $R_w =$

0.023). The promolecule consisted of neutral isolated Hartree–Fock atoms or contracted spherical H atoms with fixed neutron values for all atomic positional parameters and for H-atom thermal parameters. Electron population parameters were determined for charge deformations up to octapoles (quadrupoles for H atoms). The zwitterion is strongly polarized with a calculated dipole moment of 13 (2) debye

(1 debye $\equiv 3.34 \times 10^{-30}$ C m) at an angle 22° with the crystal b axis. In the C–O–P–O–H system, both O atoms have a planar trigonal rather than a tetrahedral disposition of deformation density. The ester O atom, which would be favored as H-bonding acceptor in an isolated molecule, is not H bonded in the crystal. In maps of electrostatic potential for three molecules arranged as in the crystal structure, the negative potential at this O atom is cancelled because of nearby polar groups. A layer of zwitterions from the crystal structure may provide a model for the outer surface of a phospholipid bilayer. Sections parallel to the layer show a checkerboard pattern of positive and negative regions of electrostatic potential. There are differences from the results obtained for a similar layer derived from the crystal structure of a phosphatidylethanolamine.

Introduction

Phosphorylethanolamine (2-aminoethyl phosphate, PEA; Fig. 1) has biological importance since it forms the polar head-group of certain phospholipids. In the crystal structure, the molecule exists as a zwitterion and has a folded conformation (Kraut, 1961). In connection with the present charge density studies, the neutron crystal structure has been determined at 122 K (Weber, McMullan, Swaminathan & Craven, 1984, hereafter WMSC). The earlier crystal structure determination by Kraut (1961) was at room temperature.

Experimental

In the X-ray refinement of Kraut (1961), six strong reflections at small $\sin \theta / \lambda$ values were omitted because of apparent severe extinction effects. In the neutron structure determination (WMSC) the extinction, although not severe, was found to be significantly anisotropic. Thus, we attempted to modify the texture of the crystals used for the X-ray data collection, hoping this would minimize extinction.

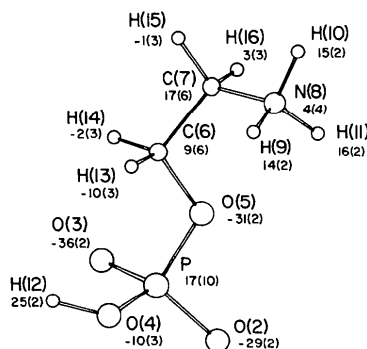


Fig. 1. Atomic nomenclature (as in Kraut, 1961) and net charges (electrons $\times 100$) for each pseudoatom. The PEA zwitterion is shown in the crystal conformation.

Crystals of PEA, grown by slowly evaporating a saturated aqueous solution, were sealed in thin quartz ampules and subjected to radiation damage at the Medical Reactor Facility, Brookhaven National Laboratory. The sample was in a water-filled can with Cd shielding to reduce the flux of thermal neutrons. The irradiating flux was estimated to be 9×10^7 neutrons $\text{mm}^{-2} \text{s}^{-1}$. The crystal selected for X-ray data collection was subjected to irradiation for 15 min and later to thermal shock by repeated dipping into liquid nitrogen. However, the X-ray data from this crystal were found to be unsatisfactory for a charge density study, presumably because of the excessive number of defects which had been introduced. There was a highly significant ($>10\sigma$) expansion of 0.032 \AA in the c lattice parameter at 123 K. Also, in the final difference Fourier synthesis, the P atom occurred at a deep minimum in the electron density, -1.2 e \AA^{-3} , surrounded by a shell of electron density 1.4 e \AA^{-3} at a distance of 0.5 \AA . No effort was made to explain these effects in detail. The data were recollected using a crystal not subjected to high-energy neutrons or to thermal shock.

X-ray data collection: Enraf–Nonius CAD-4 diffractometer, Nb-filtered $\text{Mo } K\alpha$ radiation ($\lambda = 0.7107 \text{ \AA}$); crystal $0.22 \times 0.20 \times 0.28 \text{ mm}$ mounted with the $(\bar{1}02)$ reciprocal-lattice vector close to the φ axis of the diffractometer; crystal cooled to $123 \pm 2 \text{ K}$ by a stream of nitrogen gas from an Enraf–Nonius low-temperature device; temperature measured with a thermocouple at a distance 8 mm upstream from the crystal.

The crystal lattice parameters were obtained by a least-squares fit of $\sin^2 \theta$ values for 60 reflections measured at $\pm \theta$ in the range $19^\circ < |\theta| < 26^\circ$. At 123 K, the measured cell parameters (compared with WMSC values in square brackets) are $a = 9.014$ (2) [9.015 (1)], $b = 7.751$ (2) [7.745 (1)], $c = 8.792$ (2) [8.788 (2)] \AA and $\beta = 102.43$ (2) [102.51 (1)] $^\circ$. The crystals have space group $P2_1/c$ with four molecules per cell.

The intensities with $\sin \theta / \lambda < 1.0 \text{ \AA}^{-1}$ were measured for one quadrant of reciprocal space, using $\omega/2\theta$ scans of width $\Delta 2\theta = (2.2 + 0.70 \tan \theta)^\circ$. Also, 496 reflections with $1.0 < \sin \theta / \lambda < 1.3 \text{ \AA}^{-1}$ were measured, selected because the normalized structure amplitude calculated from the nuclear parameters (WMSC) gave $|E_{hkl}| > 2.5$. The range of scan time was 120 to 180 s/reflection. Integrated intensities were estimated from the scan profiles which were each recorded at 96 equal intervals. For most reflections this was carried out using the Lehmann–Larsen algorithm as modified by Blessing, Coppens & Becker (1974). The profiles were analyzed individually for weak reflections where the automated procedure failed and for all reflections with $\theta < 7^\circ$ where we used the method of Nelmes (1975). The intensities were corrected for X-ray absorption ($\mu = 3.81 \text{ cm}^{-1}$)

using a Gaussian approximation (Busing & Levy, 1957). The variance in an integrated intensity was obtained from $\sigma^2(I) = \sigma^2 + s^2(k)I_o^2 + k^2p^2I_o^2$ (McCandlish, Stout & Andrews, 1975) where σ^2 is the variance due to counting statistics, $s^2(k) = 0.00039$ is the variance in the scale factor ($k = 1$ in this case) and $p = 0.0118$ is the instability constant. Values of s and p were calculated from the variation in the intensities of the three monitor reflections which were measured after every 50 reflections during data collection. The expression for the variance thus becomes $\sigma^2(I) = \sigma^2 + (0.023I)^2$. A total of 5587 independent reflections were measured, but only the 4150 reflections with $|F_o| \geq 3\sigma(F)$ were used in the structure refinement.

The electronic charge density was determined by least-squares refinement based on the rigid pseudoatom model of Stewart (1976). Each pseudoatom is assumed to have an invariant core component consisting of an isolated neutral Hartree-Fock atom with anomalous dispersion (Cromer, Waber & Ibers, 1974), or a spherically averaged bonded neutral H atom (Stewart, Davidson & Simpson, 1965). The variable component which describes the net charge and asphericity of the pseudoatom consists of terms, each involving a Slater-type radial function and a multipole angular function, weighted by an electron population parameter. The multipole expansion is taken up to octapoles for C, N, O, P, quadrupoles for H. For C, N, O and H, the explicit functions were those given by Epstein, Ruble & Craven (1982), assuming radial exponents with fixed values $\alpha = 3.2, 3.9, 4.5$ and 2.4 bohr^{-1} respectively (the Bohr radius is 52.92 pm). For P, assuming $n = 4$, the radial scattering factors are $f_b = (1 + c^2)^{-6} [1 - 3.3333c^2 + c^4]$, $f_d = c(1 + c^2)^{-6} [0.2333 - 2.8c^2 + 0.2c^4]$, $f_g = c^2(1 + c^2)^{-6} [3.7333 - 1.6c^2]$, and $f_o = c^3(1 + c^2)^{-6} \times [4.80 - 0.5333c^2]$, where $c = s/\alpha$, $s = \sin \theta/\lambda$, and α is estimated to be 3.2 bohr^{-1} .*

Fixed WMSC neutron diffraction values were assumed for all atomic positional parameters and for H-atom anisotropic thermal parameters. In addition to the population parameters, the structure model included the usual overall scale factor, the anisotropic thermal parameters and an isotropic extinction factor of type I with Lorentzian crystal mosaicity (Becker & Coppens, 1974), giving a total of 250 variables. The least-squares refinement was carried out by the computer program of Craven & Weber (1981). The function minimized was $\sum w\Delta^2$, where $\Delta = |F_o| - |F_c|$ and $w = \sigma^{-2}(F_o)$. Convergence was obtained with $R =$

0.029 , $R_w = 0.023$ and $S = 1.20$.* Although the net charge for the PEA zwitterion should be zero, the value obtained from the sum of monopole population parameters is $-1.94(16) \text{ e}$. Since there are 74 electrons in the molecule, the model accounts for 97.4% of the total. A difference Fourier synthesis (Fig. 2a) showed small but significant (4σ) residual features near O(5) and the P atom. Since they were absent when the calculations included only reflections with $\sin \theta/\lambda \leq 0.7 \text{ \AA}^{-1}$, it is concluded that they come from the region of electron density close to the O(5) and P nuclei. No satisfactory distinction can be made whether these residual features are due to an inadequacy in the model for the static charge density distribution, or for the thermal vibrations. However, in a second refinement, we have shown that these features become insignificant (Fig. 2b) when third-order thermal parameters for non-H atoms are included. Because of the marginal improvement in agreement,† the parameters which we report (Tables 1 and 2) and use for charge density and electrostatic potential mapping are from the first refinement.‡ Electron population parameters include a scale factor of 1.04, so that the molecule becomes electrically neutral.

The differences ΔU_{ij} between thermal parameters determined by X-ray (Table 1) and neutron diffraction (Table 2 in WMSC) are within experimental error

$$* R = \sum |\Delta| / \sum F_o; \quad R_w = (\sum w\Delta^2 / \sum wF_o^2)^{1/2}; \quad S = [\sum w\Delta^2 / (n_o - n_p)]^{1/2}.$$

† The agreement criteria become $R = 0.028$, $R_w = 0.022$ and $S = 1.16$. Eight of the 80 c_{jkl} values are significantly different ($>3\sigma$) from zero, the largest being $-94(18) \times 10^{-7}$ for c_{333} of atom O(2). There were no significant changes in U_{ij} values and only marginally significant changes ($<2\sigma$) in population parameters.

‡ Lists of structure factors and the electron population parameters have been deposited with the British Library Lending Division as Supplementary Publication No. SUP39380 (46 pp.). Copies may be obtained through The Executive Secretary, International Union of Crystallography, 5 Abbey Square, Chester CH1 2HU, England.

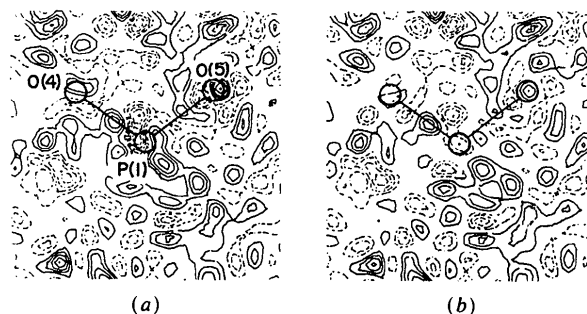


Fig. 2. Fourier synthesis of residual electron density in the O(4)-P-O(5) plane. Contours are at 0.05 e \AA^{-3} with the zero contour omitted. E.s.d.'s are 0.11 e \AA^{-3} at the P atom, 0.06 e \AA^{-3} elsewhere. (a) After first refinement. (b) After second refinement, including third-order thermal parameters.

* The α value for P was obtained by minimizing the residual $\sum_{l=0}^4 (f_{P,l} - f_{m,l})^2$ where $f_{P,l}$ is the generalized scattering factor for P in one of the diatomics P_2 , PH, PO, PF and PN as determined by R. F. Stewart (private communication), and $f_{m,l}$ is calculated assuming the multipole model. The five values ranged from $\alpha = 3.43$ (PN) to 2.84 bohr^{-1} (P_2).

Table 1. Anisotropic thermal parameters ($\text{\AA}^2 \times 10^4$)

Temperature factors have the form $T = \exp[-2\pi^2 \sum_i \sum_j h_i h_j a_i^* a_j^* U_{ij}]$. Values of U_{ij} are from the X-ray refinement which did not include third-order temperature factors. Values of U_{ij} assumed for the H atoms are in Table 2 of WMSC.

	U_{11}	U_{22}	U_{33}	U_{12}	U_{13}	U_{23}
P	72 (1)	90 (1)	115 (1)	-7 (1)	-3 (1)	4 (1)
O(2)	113 (2)	108 (2)	299 (3)	1 (2)	-40 (2)	37 (2)
O(3)	111 (2)	215 (2)	142 (2)	-11 (2)	15 (1)	-58 (2)
O(4)	123 (2)	339 (3)	124 (2)	-49 (2)	15 (2)	35 (2)
O(5)	122 (2)	95 (2)	203 (2)	0 (1)	-23 (2)	1 (2)
C(6)	139 (2)	111 (2)	182 (2)	11 (1)	-25 (2)	-1 (2)
C(7)	199 (2)	113 (2)	143 (2)	3 (2)	0 (2)	14 (2)
N(8)	118 (2)	103 (2)	145 (2)	4 (1)	19 (2)	4 (2)

Table 2. Electron population parameters

(a) Atomic axial system

Values are referred to a right-handed Cartesian set of local axes with $x = \mathbf{u}$, $z = \mathbf{u} \times \mathbf{v}$ and $y = \mathbf{x} \times \mathbf{z}$, where \mathbf{u} and \mathbf{v} are bond vectors for each atom as defined below.

	\mathbf{u}	\mathbf{v}	\mathbf{u}	\mathbf{v}
P	O(2)-O(3)	O(4)-O(5)	H(9)	H(9)-N(8)
O(2)	O(2)-P	O(2)-O(3)	H(10)	H(10)-N(8)
O(3)	O(3)-P	O(3)-O(2)	H(11)	H(11)-N(8)
O(4)	O(4)-P	O(4)-O(5)	H(12)	H(12)-O(4)
O(5)	O(5)-P	O(5)-C(6)	H(13)	H(13)-C(6)
C(6)	H(13)-H(14)	O(5)-C(7)	H(14)	H(14)-C(6)
C(7)	H(15)-H(16)	C(6)-N(8)	H(15)	H(15)-C(7)
N(8)	H(9)-H(10)	C(7)-H(11)	H(16)	H(16)-C(7)

Table 2 (cont.)

(b) Parameter values (electrons $\times 10^2$)

Values were first normalized as described in the Appendix of Epstein, Ruble & Craven (1982), and then multiplied by 1.04 to give a neutral molecule.

	p_v	d_1	d_2	d_3	q_1	q_2	q_3	q_4	q_5	o_1	o_2	o_3	o_4	o_5	o_6	o_7
P	-17 (10)	10 (4)	29 (4)	16 (4)	-12 (3)	-4 (2)	-3 (2)	1 (2)	-1 (2)	-5 (2)	-2 (2)	62 (2)	2 (2)	4 (2)	0 (2)	-8 (2)
O(2)	29 (2)	-3 (1)	3 (1)	0 (1)	3 (2)	-1 (2)	-3 (2)	3 (2)	-1 (2)	1 (1)	-2 (1)	1 (1)	-1 (1)	-1 (1)	2 (1)	3 (1)
O(3)	36 (2)	-2 (1)	-1 (1)	2 (1)	-1 (2)	0 (2)	4 (2)	-1 (2)	-3 (2)	1 (1)	-2 (1)	1 (1)	-2 (1)	-1 (1)	0 (1)	-2 (1)
O(4)	10 (3)	1 (1)	0 (1)	9 (1)	-2 (2)	4 (2)	-4 (2)	-2 (2)	-2 (2)	1 (1)	-1 (1)	1 (1)	-6 (1)	-7 (1)	4 (1)	-2 (1)
O(5)	31 (2)	-1 (1)	-7 (1)	2 (1)	2 (2)	2 (2)	0 (2)	-1 (2)	4 (2)	6 (1)	1 (1)	1 (1)	-2 (1)	3 (1)	-3 (1)	0 (1)
C(6)	-9 (6)	0 (2)	9 (2)	-6 (2)	2 (2)	1 (2)	-5 (2)	5 (2)	2 (2)	3 (2)	4 (2)	-31 (2)	-1 (2)	-1 (2)	1 (2)	-4 (2)
C(7)	-17 (6)	-4 (2)	-4 (2)	-1 (2)	2 (2)	-2 (2)	4 (2)	-5 (2)	0 (2)	0 (2)	0 (2)	-33 (2)	0 (2)	1 (2)	-2 (2)	-7 (2)
N(8)	-4 (4)	2 (1)	-1 (1)	-2 (1)	2 (2)	-1 (2)	-2 (2)	0 (2)	2 (2)	1 (1)	4 (1)	-19 (2)	-2 (2)	0 (1)	5 (1)	1 (2)
H(9)	-14 (2)	20 (2)	1 (2)	4 (2)	7 (3)	-2 (2)	-3 (3)	0 (2)	-7 (2)							
H(10)	-15 (2)	13 (2)	2 (2)	1 (2)	9 (3)	2 (3)	2 (2)	1 (2)	-14 (2)							
H(11)	-16 (2)	21 (2)	3 (2)	-2 (2)	17 (3)	0 (2)	-6 (3)	0 (2)	-14 (2)							
H(12)	-25 (2)	23 (2)	-2 (2)	-2 (2)	23 (3)	7 (2)	4 (3)	-4 (2)	-10 (2)							
H(13)	10 (3)	16 (2)	-6 (2)	0 (2)	10 (3)	-4 (3)	-2 (3)	-2 (2)	-9 (3)							
H(14)	2 (3)	16 (2)	1 (2)	4 (2)	9 (3)	-2 (3)	13 (3)	-2 (3)	-6 (3)							
H(15)	1 (3)	16 (2)	-8 (2)	-3 (2)	1 (3)	1 (3)	0 (3)	2 (2)	-5 (3)							
H(16)	-3 (3)	22 (3)	1 (2)	-2 (2)	13 (3)	-5 (3)	-1 (3)	-4 (2)	-6 (3)							

($<3\sigma$) except for U_{11} and U_{33} for P, U_{22} for O(3) and O(4), and U_{33} for N(8).^{*} The X-ray values are systematically larger for the lighter atoms and smaller for the P atom.

Maps of the deformations in the charge density, including monopole terms (Figs. 3 and 4), were calculated using the computer programs of Craven & Weber (1981). They are based on a stationary arrangement of pseudoatoms with charge density terms in crystal space as given by Epstein *et al.* (1982). Maps of the total electrostatic potential (Figs. 5 and 6) were calculated with these programs as modified by He (1983). They include contributions from the atomic nuclei and the electrons of the invariant core, assuming the wavefunctions tabulated by Clementi (1965).

Discussion

The net charge for each pseudoatom (Fig. 1) is the monopole population parameter with opposite sign ($-p_v$, Table 2) so that a negative net charge represents an excess of electrons. It must be remembered that these values depend on the assumed model, particularly the radial exponent α , so that comparisons of net charges are most reliable for pseudoatoms of

the same kind. Thus, the chemically equivalent phosphoryl oxygen atoms O(2) and O(3) have similar net charges $[-0.29, -0.36 (2) e]$ of magnitude significantly greater than for the hydroxyl O(4) $[-0.10 (3) e]$. There is also a considerable negative charge $[-0.31 (2) e]$ on the ester oxygen O(5). Whereas the methylene H atoms are almost neutral with charges ranging from $-0.03 (3)$ to $+0.10 (3) e$, the ammonium H atoms carry a positive charge $[0.14, 0.15, 0.16 (2) e]$ and the hydroxyl H atom is even more positively charged $[+0.25 (2) e]$. The electropositivity of those H atoms involved in H bonding is a distinctive feature which has been noted in other charge density studies (Craven & Benci, 1981; Epstein *et al.*, 1982; Craven & Weber, 1983).

The charge distribution in PEA (Fig. 1) has zwitterionic character with the phosphate negative $[-0.64 (11) e]$ and the ammonium group positive $[+0.49 (5) e]$. We attribute the folded conformation of the molecule to the Coulombic attraction between these groups. The molecular dipole moment calculated as outlined by Stewart (1972) is 13 (2) debye (1 debye $\equiv 3.34 \times 10^{-30} \text{ C m}$) and makes an angle of 22° with the crystal b axis. For the zwitterion γ -aminobutyric acid (Craven & Weber, 1983) a similar charge separation was obtained $[+0.57 (3)$ and $-0.59 (4) e]$ with molecular dipole moment 13 (1) debye.

^{*} The most significant difference is $\Delta U_{33} = 0.0016 (2) \text{\AA}^2$ for P.

In the ethylammonium group of PEA, the principal deformations of the charge density are tetrahedral at the N and C atoms and dipolar at the H atoms, with electron population parameters (Table 2) similar to those obtained for the corresponding group in γ -aminobutyric acid (Craven & Weber, 1983).

The phosphate group has deformation charge density with approximate local mirror symmetry in the section through O(2)–P–O(3) (Fig. 3*a*). This is expected because of the chemical equivalence of the phosphoryl atoms O(2) and O(3), and their similar crystal environments. Both O atoms have excess electron density in the region where they form intermolecular H bonds. For O(3), there are two H bonds close to the plane of Fig. 3*a*). There are also two H bonds at O(2), which are better seen in Fig. 4*a*).

In contrast to Fig. 3*a*), the section through the other two O atoms (Fig. 3*b*) lacks local symmetry. From Table 2, it is seen that the asphericity of the P atom is largely due to a single deformation term (o_3). Because of its tetrahedral symmetry, this term contributes electron density almost equally to the σ region of each P–O bond. However, there is also an

important dipole deformation at the P atom [$d = 0.35(7)$, the resultant of d_1 , d_2 and d_3 in Table 2] making an angle 25° with the P–O(4) bond. Thus the P–O(4) bond differs from the other P–O bonds in that electronic charge is displaced from the σ -bond region of the P–O(4) bond to the opposite side of the P atom, reducing the magnitude of the negative peak which occurs there. The resulting difference in bond character between P–O(4) and P–O(5) may arise because of conformational differences about the adjacent bonds. The bond O(5)–C(6) has the usual staggered conformation in the view along P–O(5), whereas in the view along P–O(4), the bond O(4)–H(12) almost eclipses the bond P–O(3).^{*} Atoms O(4) and O(5), neither of which accepts an H bond, each have a single lobe of non-bonding density $0.71(10) e \text{ \AA}^{-3}$ occurring in the planes P–O(4)–H(12) and P–O(5)–C(6) respectively (Fig. 4). Thus the asphericity of O(4) and O(5) has trigonal rather than tetrahedral character. Similar trigonal deformations occur at the hydroxyl O atoms of the H_2PO_4 ion in putrescine diphosphate (Takusegawa & Koetzle, 1979) and in the quartz-like structure of AlPO_4 (Thong & Schwarzenbach, 1979) where the O atoms all form two bonds due to the corner sharing of AlO_4 and PO_4 tetrahedra.

There is nothing extraordinary in the O–H...O and N–H...O H bonds in PEA. As shown in Fig. 4, the strong dipole deformation at each H atom transfers electronic charge into the O–H or N–H bond, thus deshielding the proton with respect to the acceptor atom and contributing to an attractive electrostatic interaction.

In considering the H bonding in the crystal structure, our attention turned to the ester linkage atom O(5), since this is the only phosphate O atom which appears not to be involved.[†] This distinction in the behavior of atom O(5) is not due to its reduced electronegativity, since, as noted above, the ester O atom has almost the same net charge as the two phosphoryl O atoms, O(2) and O(3). We inspected the deformation density near O(5) but could find no polarization of the non-bonding lobe which could be

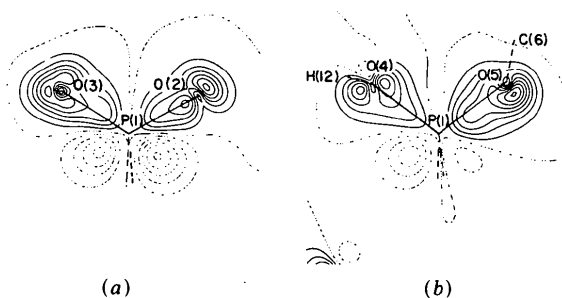


Fig. 3. Deformation charge density for a static atomic arrangement. Contours are at intervals of $0.10 e \text{ \AA}^{-3}$ with zero and negative contours shown as broken lines. E.s.d.'s are $0.1 e \text{ \AA}^{-3}$ near O atoms and $0.05 e \text{ \AA}^{-3}$ in the bond regions. (a) Section through atoms O(2), P, O(3). (b) Section through atoms O(4), P, O(5). Atoms H(12) and C(6) are on opposite sides of this section.

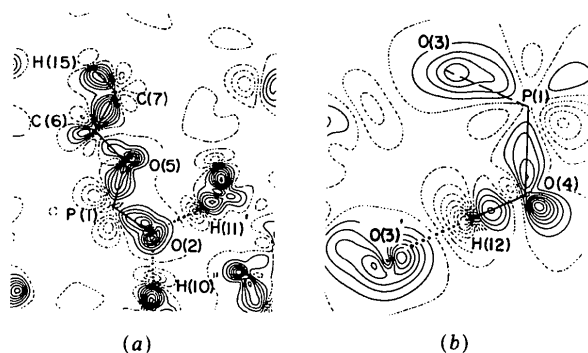
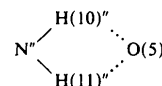


Fig. 4. Deformation charge density for a static atomic arrangement, contours as in Fig. 3. (a) Section in the best least-squares plane through atoms O(2), P, O(5), C(6), C(7) and H(15). This is close to the plane of the H bonds at O(2). (b) Section through atoms P, O(4) and H(12). This is close to a center of symmetry and to atom O(3)'.

^{*} Torsion angles C(6)–O(5)–P–O(4), H(12)–O(4)–P–O(5) and H(12)–O(4)–P–O(3) are $-61.6(1)$, $100.0(1)$ and $-17.6(1)^\circ$ respectively (Table 4, WMSC). The near eclipsing of O(4)–H(12) and P–O(3) allows PEA molecules related by a center of symmetry to form pairs of strong H bonds, with distances H(12)...O(3)' of $1.535(1) \text{ \AA}$.

[†] According to the neutron diffraction results (WMSC), the shortest H...O(5) distance which might be considered an H bond occurs in the intramolecular interaction, N–H(11)...O(5). However, the H...O distance (2.76 \AA) is greater than the sum of van der Waals radii (2.6 \AA) and the N–H...O angle is acute (85.4°). The next shortest are the intermolecular interactions



(Fig. 4*a*), with H...O distances 3.06 , 2.87 \AA and N–H...O angles 102.9 , 115.2° for H(10)' and H(11)' respectively.

interpreted as an intramolecular interaction with the closest ammonium atom H(11). We then used the pseudoatom model with population parameters from Table 2 in order to calculate the electrostatic potential for a PEA zwitterion removed from the lattice. This was performed in the same section as the deformation density (Fig. 4a). We expected that the positive potential from the ammonium group would neutralize the negative potential near O(5), thus making O(5) less attractive to an approaching H-bonding proton. However, an opposite effect is observed (Fig. 5b). Due to contributions from the other O atoms, the region near O(5) is found to have the minimum electrostatic potential in this section [$-0.28(5) \text{ e } \text{Å}^{-1}$ or $-390(71) \text{ kJ mol}^{-1}$] ($1 \text{ e } \text{Å}^{-1} \equiv 1390 \text{ kJ mol}^{-1}$). Thus if steric effects are neglected, the H bonding of an isolated PEA molecule should occur with O(5) slightly favored over O(2) as the acceptor atom. We continued by mapping the electrostatic potential with a second and a third molecule introduced stepwise. These molecules form the two H bonds at O(2) as they occur in the crystal structure (Fig. 4a). The third molecule contains the ammonium group which makes the two closest intermolecular H \cdots O(5) distances in the crystal.* As seen in Figs. 5(c) and 5(d), the second molecule has little effect on the electrostatic potential near O(5), but the third reduces it almost to zero.

* See previous footnote.

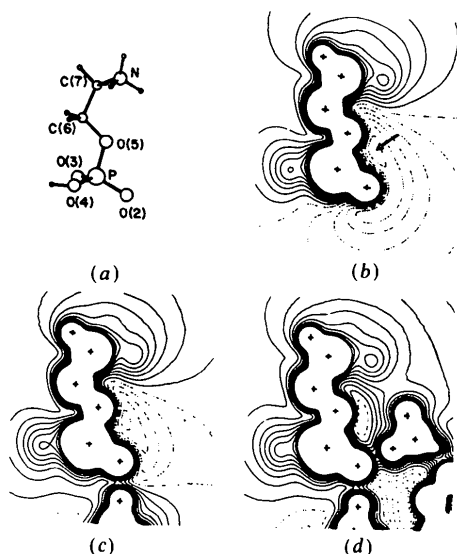


Fig. 5. The total electrostatic potential for PEA in same section as Fig. 4(a). Contours are at intervals $0.05 \text{ e } \text{Å}^{-1}$ with zero and negative contours as broken lines. For a unit positive charge as probe, the potential is a minimum in the negative regions. (a) Molecule in the orientation used for mapping. (b) Isolated molecule. The minimum potential [$-0.28(5) \text{ e } \text{Å}^{-1}$, see arrow] is near O(5), which is not H bonded in the crystal structure. (c) A second molecule is introduced, forming the N-H(10) \cdots O(2) interaction as in the crystal structure. There is little effect on the potential near O(5). (d) A third molecule is introduced, forming the second H bond at O(2) (see Fig. 4a). Although O(5) is not H bonded, the potential nearby becomes almost zero.

This stepwise sequence is not presented as a realistic pathway for crystal nucleation because it occurs in vacuum with PEA molecules at infinite dilution. Also the crystal configuration has been preserved with no effort to minimize the energy of molecular interaction. However, we believe these maps are interesting because they show that the intrinsic H-bonding capacity of atom O(5) could be satisfied indirectly, as a consequence of nearby interactions among other polar groups. It is worth emphasizing that, because of the $1/r$ dependence of the electrostatic potential, H-bonding interactions may have long-range effects, extending beyond the particular donor and acceptor atoms.

The electrostatic potential has also been mapped for a layer of PEA zwitterions which might be considered as a model for the polar surface of a phospholipid bilayer. These calculations were carried out upon noticing a close relationship between the crystal structure of PEA and the polar region in the crystal structure of the acetic acid solvate of 1,2-dilauroyl-DL-phosphatidylethanolamine (Hitchcock, Mason, Thomas & Shipley, 1974). In the phospholipid crystal structure, which also has the space group $P2_1/c$, the molecules form lipid bilayers with the diglyceride groups at the center and closely packed PEA groups on the outer surfaces. The repeating unit for each outer surface has the orthogonal crystal lattice translations $b = 7.77$, $c = 9.95 \text{ Å}$ and contains two PEA groups. They are oriented with their long axes nearly parallel to the layer surface and are related by the c -glide plane. A similar molecular arrangement is obtained from the crystal structure of PEA by dissecting out the molecular layer contained between the lattice planes $x = 0$ and $x = \frac{1}{2}$ (see Fig. 1, WMSC).^{*} Lattice translations for this layer are $b = 7.75$, $c = 8.79 \text{ Å}$ at 123 K, indicating a closer packing than in the phospholipid structure. However, the two-dimensional network of N-H \cdots O H bonds is the same. The formation of an isolated layer from the PEA structure (Fig. 6a) requires breaking the H bonds N-H(11) \cdots O(2) on one side and O(4)-H(12) \cdots O(3) on the other. Supposedly, the layer could then be converted to phospholipid by substituting diglyceride groups at the projecting H(12) atoms which are labelled R in Fig. 6(a).

The electrostatic potential has already been calculated for an isolated monolayer taken from the phospholipid crystal structure (Zakrzewska, Lavery & Pullman, 1981). The necessary charge distribution was derived from *ab initio* wavefunctions calculated for each of four fragments within the isolated molecule. With some approximations, this enabled the electrostatic potential to be mapped, except within

* No such arrangement can be derived from the crystal structure of *O*-(1- α -glycerylphosphoryl)ethanolamine monohydrate (De Titta & Craven, 1973).

the molecular envelope 2 \AA from each atomic nucleus. For the isolated molecule, the minimum potential (-274 kJ mol^{-1}) is found near the phosphoryl O atoms.* In our experimental map for an isolated PEA zwitterion, the minimum is in the same region, but it is somewhat deeper [$-432 (67) \text{ kJ mol}^{-1}$]. Better agreement for this kind of comparison has been obtained in the case of imidazole (Stewart, 1982), where the minimum electrostatic potential near atom

* Meaningful comparison of maximum values cannot be made because of the rapid increase in the potential at decreasing distance from each atomic nucleus.

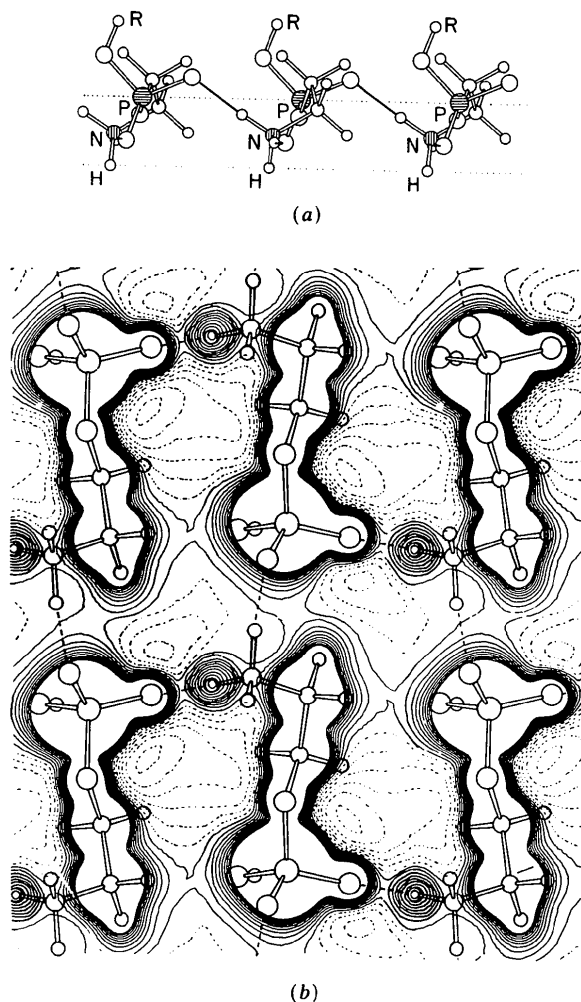


Fig. 6. Total electrostatic potential for a monolayer of PEA zwitterions, contours as in Fig. 5. (a) Molecular arrangement in the monolayer. These are the molecules contained between crystal lattice planes $0 < x < \frac{1}{2}$ in Fig. 1 of WMSC. The view is down the crystal axis b , with c from left to right. Atoms marked R are H(12), which supposedly could be substituted by diglyceride groups to form a model phospholipid layer. Dotted lines (b) and (c) through the P atoms and H(11) atoms are 2 \AA apart. They represent the trace of planes for which the electrostatic potential has been calculated. (b) Electrostatic potential in section through P atoms.

N(3) was found to be 310 and 344 kJ mol^{-1} in the theoretical and experimental maps respectively. The present discrepancies may be due to a combination of factors, such as the absence of the diglyceride in our calculations, a conformational difference between the two PEA moieties,* and the low accuracy obtained for the atomic positions in the phospholipid structure. Since the phospholipid H atoms were not located experimentally, they were introduced by Zakrzewska *et al.* (1981) at presumed positions. Possibly, there are also significant differences in the distribution of the charge density as determined experimentally and theoretically. The details of the theoretical distribution have not been described.

In Fig. 6(b, c) we show the electrostatic potential for a finite layer of 5×3 PEA zwitterions measuring $22 \times 23 \text{ \AA}$, in which both the atomic positions and the charge distribution were determined from the diffraction data. Because of computational limitations, the mapping in each section was actually restricted to an area $b \times c/2$ about the central molecule. For showing its immediate environment, this area was then used as a repeating motif. The dotted lines in Fig. 6(a), which are separated by 2 \AA , are the traces of the two sections (Fig. 6b, c). The first (Fig. 6b) passes through the P atoms and is approximately in the center of the

* The greatest conformational difference is in the torsion angle at C(6)-O(5), which is -101° in the phospholipid (Hitchcock *et al.*, 1974) and -167° in PEA (WMSC).

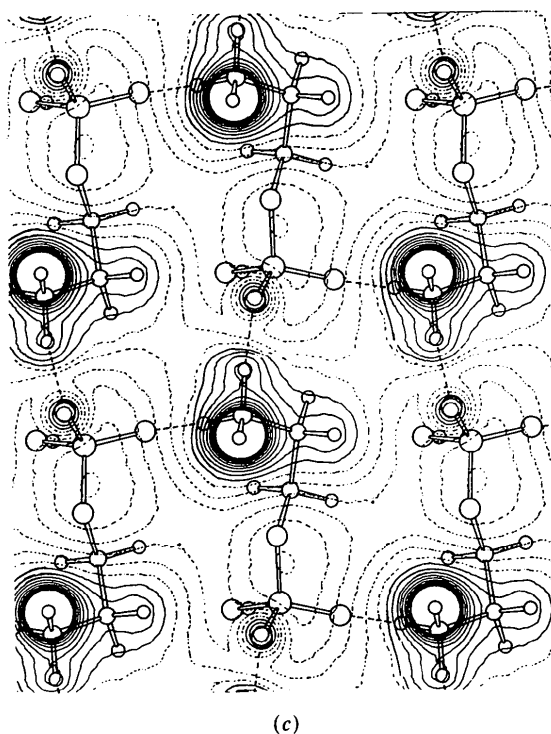


Fig. 6. (cont.). (c) Electrostatic potential in section through H(11) atoms which project from the PEA layer.

layer. The potential is negative in the intermolecular regions except for positive saddle points which occur near the midpoint of the H bond N-H...O(3) and also between the phosphate group and the C(7) methylene group. In the outer section (Fig. 6c), the predominant positive feature comes from the ammonium atom H(10). The negative regions, which are more diffuse, have a minimum $[-348 (67) \text{ kJ mol}^{-1}]$ close to atom O(5). This section is 1.5 Å from the O(5) nucleus, and hence is almost tangent to its van der Waals sphere. The distribution of the potential is simpler in Fig. 6(c) than in Fig. 6(b), with positive and negative regions forming almost a square checkerboard pattern. This pattern persists in sections at increasing distance from the molecular layers (maps not shown). In the section 1.2 Å from the H(11) nucleus, tangent to its van der Waals sphere (not shown), the maximum positive potential which occurs near H(11) is 109 kJ mol^{-1} and the minimum is $-176 (67) \text{ kJ mol}^{-1}$. In the section 2.0 Å from Fig. 6(c), these values are 17 and $-117 (67) \text{ kJ mol}^{-1}$. Thus the magnitude of the positive potential decreases more rapidly than the negative potential with increasing distance from the molecular layer.

The results for the PEA and phospholipid layers are different. Zakrzewska *et al.* (1981) report that the electrostatic potential for the phospholipid layer is predominantly positive over the surface which is defined as the envelope at 1.7 times the van der Waals radius from each atomic nucleus. The differences in electrostatic potential are consistent with the interactions observed for each layer in its crystal structure. Thus, the phospholipid layer, which should preferentially attract electronegative groups, forms an H bond N-H...O with an acetic acid O atom. The PEA layer with regions of positive and negative potential is both donor and acceptor in N-H...O H bonding. The differences in potential for these model layers may be due to differences in their structure and molecular packing.* However, as noted above in comparing the isolated molecules, other factors may be involved.

This work will be continued by using the pseudoatom model to study the likely hydration sites

* Our approximate potential calculations for a 3×5 phospholipid layer are consistent with the results of Zakrzewska *et al.* (1981). Atomic positions were those of Hitchcock *et al.* (1974) with H atoms included at presumed positions, and diglyceride groups deleted. All atoms were assigned the net charges obtained for PEA (Table 2), but no higher multipoles were included. Electrostatic potential maps showed the checkerboard pattern observed for the PEA layer, but with positive regions predominating. Values at 0.5 Å beyond the van der Waals radius of the projecting H(11) and O(3) atoms were +122 and $-21 (42) \text{ kJ mol}^{-1}$ respectively. Values reported by Zakrzewska *et al.* are +244 and -17 kJ mol^{-1} .

of the PEA layer. First the structure refinements of various crystalline hydrates must be carried out in order to obtain typical electron population parameters for the water molecules.

This work was supported by Grants GM-22548 and HL-20350 from the National Institutes of Health. We are grateful to Drs R. F. Stewart and M. A. Spackman for discussions concerned with the calculation of electrostatic potential, to Dr Xiao-min He for the modifications in the computer programs used for mapping electrostatic properties, to Dr H.-P. Weber and the staff at Brookhaven National Laboratory for the crystal irradiation experiments, and to Dr John Ruble, Mr Paul Kruth and Mrs Joan Klinger for technical assistance.

References

- BECKER, P. J. & COPPENS, P. (1974). *Acta Cryst.* **A30**, 129–147.
 BLESSING, R. H., COPPENS, P. & BECKER, P. (1974). *J. Appl. Cryst.* **7**, 480–492.
 BUSING, W. R. & LEVY, H. A. (1957). *Acta Cryst.* **10**, 180–182.
 CLEMENTI, E. (1965). *IBM J. Res. Dev. Suppl.* **9**, 2.
 CRAVEN, B. M. & BENCI, P. (1981). *Acta Cryst.* **B37**, 1584–1591.
 CRAVEN, B. M. & WEBER, H.-P. (1981). *The POP Least Squares Refinement Procedure*. Tech. Rep. Crystallography Department, Univ. of Pittsburgh.
 CRAVEN, B. M. & WEBER, H.-P. (1983). *Acta Cryst.* **B39**, 743–748.
 CROMER, D. T., WABER, J. T. & IBERS, J. A. (1974). *International Tables for X-ray Crystallography*, Vol. IV, pp. 148–151. Birmingham: Kynoch Press.
 DETITTA, G. T. & CRAVEN, B. M. (1973). *Acta Cryst.* **B29**, 1354–1357.
 EPSTEIN, J., RUBLE, J. R. & CRAVEN, B. M. (1982). *Acta Cryst.* **B38**, 140–149.
 HE, X.-M. (1983). *The MOLPOT Computer Program*. Tech. Rep. Crystallography Department, Univ. of Pittsburgh.
 HITCHCOCK, P. B., MASON, R., THOMAS, K. M. & SHIPLEY, G. G. (1974). *Proc. Natl Acad. Sci. USA*, **71**, 3036–3040.
 KRAUT, J. (1961). *Acta Cryst.* **14**, 1146–1152.
 MCCANDLISH, L. E., STOUT, G. H. & ANDREWS, L. C. (1975). *Acta Cryst.* **A31**, 245–249.
 NELMES, R. J. (1975). *Acta Cryst.* **A31**, 273–279.
 STEWART, R. F. (1972). *J. Chem. Phys.* **57**, 1664–1668.
 STEWART, R. F. (1976). *Acta Cryst.* **A32**, 565–574.
 STEWART, R. F. (1982). *God. Jugosl. Cent. Krystalogr.* **17**, 1–24.
 STEWART, R. F., DAVIDSON, E. R. & SIMPSON, W. T. (1965). *J. Chem. Phys.* **42**, 3175–3187.
 TAKUSAGAWA, F. & KOETZLE, T. F. (1979). *Acta Cryst.* **B35**, 867–877.
 THONG, N. & SCHWARZENBACH, D. (1979). *Acta Cryst.* **A35**, 658–664.
 WEBER, H.-P., MCMULLAN, R. K., SWAMINATHAN, S. & CRAVEN, B. M. (1984). *Acta Cryst.* **B40**, 506–511.
 ZAKRZEWSKA, K., LAVERY, R. & PULLMAN, B. (1981). *Int. J. Quantum Chem.: Quantum Biol. Symp.* **8**, 161–170.